JOURNAL OF GUIDANCE, CONTROL, AND DYNAMICS
Vol. 27, No. 1, January–February 2004

Engineering Notes

ENGINEERING NOTES are short manuscripts describing new developments or important results of a preliminary nature. These Notes cannot exceed 6 manuscript pages and 3 figures; a page of text may be substituted for a figure and vice versa. After informal review by the editors, they may be published within a few months of the date of receipt. Style requirements are the same as for regular contributions (see inside back cover).

Nonlinear Adaptive Control for Slewing Flexible Active Structures

D. G. Wilson*
Sandia National Laboratories, Albuquerque, New Mexico 87185
G. P. Starr†
University of New Mexico, Albuquerque, New Mexico 87131
G. G. Parker‡
Michigan Technological University, Houghton, Michigan 49931
and
R. D. Robinett§
Sandia National Laboratories, Albuquerque, New Mexico 87185

I. Introduction

THE development of lightweight flexible structures that include both advanced control and active material will impact several space application areas. The application of composite material technology for fabricating lightweight structures has the potential to reduce weight and improve performance at the cost of increased deflection and vibration. One way to reduce vibration is the combination of advanced control methods such as nonlinear adaptive control plus active structure technology. Active structures with both sensors and actuators, strategically placed along the structure, can suppress vibrations and enhance slewing performance.

Several advanced control strategies have been reported in the literature for slewing flexible structures with both motor torque and piezoceramic strain actuation as control inputs. Inman et al.[1] demonstrated that, by introducing an active structure, slewing control performance was improved and maximum tip deflection reduced. A standard linear quadratic regulator control design was used for the multi-input slewing control problem. Denoyer and Kwak[2] presented dynamic modeling and vibration suppression experimental results for a slewing flexible structure with surface bonded piezoceramic sensors and actuators. Several different controller designs were investigated based on positive position feedback and a multi-input/multi-output linear quadratic Gaussian design. Significant vibration suppression at the end of the slewing maneuver was achieved for these controller designs. Most recently, Choi and Shin[3] presented a novel hybrid actuator scheme to control actively and robustly the endpoint position of a flexible single-link manipulator. The control scheme consisted of two actuators: a motor mounted at the beam hub and a piezoceramic bonded to the surface of the flexible aluminum link. Sliding mode control was used to slew the beam while a constant amplitude feedback control was used to suppress actively beam vibrations. High-performance characteristics were demonstrated experimentally.

Slotine and Li[4] first introduced passivity concepts for adaptive control of rigid manipulators. Lewis et al.[5] provide a detailed overview of various control algorithms for rigid robot manipulators. In both Refs. 4 and 5, a robustness term is introduced to supress distrubances. Yang et al.[6,7] built on the nonlinear adaptive control in Ref. 4 to include passive flexible link manipulators. They recast the manipulator equations into an output measurement space and introduced a V-shaped Lyapunov function to provide a general stability proof for the flexible modes. Their algorithm only uses motor torque input at the hub with a correction term to minimize and/or cancel flexible mode oscillations.

The main contribution of our paper is the experimental evaluation of a modified nonlinear adaptive control (NAC) architecture[8] on a single-link flexible manipulator. For multilink flexible manipulators, the nonlinear dynamic terms are integrally included in the NAC design and are compensated. The NAC is a combination of the adaptive control development in Ref. 4 with the output measurement space in Ref. 6 that introduces flexible link actuation.[9] In this development, control laws are developed for both motor torque control and beam vibration control actuation. In addition, a tracking error sliding surface is defined that includes the addition of an integral term. This algorithm can be successfully applied to both direct-drive and geared or harmonic-drive flexible manipulators. The reference angles and rates are based on near-minimum-time maneuvers of an equivalent rigid system. The NAC algorithm uses output sensor data from the encoder and strain sensor along with rate estimation to compute the control input for both the motor and strain actuators. Large-angle slewing is realized with a single-axis motor drive assembly. Active vibration suppression is accomplished with a graphite/epoxy composite structure that includes embedded strain sensors and actuators. The tip mass was varied to evaluate control system robustness. Experimental slewing studies were performed to compare the benefits of using active rather than passive structures. For the active case, the experimental results showed a reduction in residual vibration and settling time. Although not a focus of this work, our method could be applied to a wider class of active structures.

II. Dynamic Model Description

The dynamics for a general multibody flexible manipulator with n_r rigid modes, n_f orthogonal flexible modes, motor torque, and piezoceramic patch actuators is given[7,8] as

$$\boldsymbol{M}(\boldsymbol{q})\ddot{\boldsymbol{q}} + \boldsymbol{C}(\boldsymbol{q}, \dot{\boldsymbol{q}})\dot{\boldsymbol{q}} + \boldsymbol{D}\dot{\boldsymbol{q}} + \boldsymbol{K}\boldsymbol{q} + \boldsymbol{\tau}_d = \begin{bmatrix} \boldsymbol{I} & \boldsymbol{0} \\ \boldsymbol{0} & \boldsymbol{b} \end{bmatrix} \begin{Bmatrix} \boldsymbol{\tau} \\ \boldsymbol{V}_{\text{piezo}} \end{Bmatrix} \quad (1)$$

where $\boldsymbol{q} = [\boldsymbol{q}_r \quad \boldsymbol{q}_f]^T$ represents the joint angles and flexible modes, respectively, $\boldsymbol{M}(\boldsymbol{q})$ is the positive definite symmetric mass matrix, $\boldsymbol{C}(\boldsymbol{q}, \dot{\boldsymbol{q}})$ is the Coriolis and centripetal matrix, $\boldsymbol{D}$ is the damping matrix, $\boldsymbol{K}$ is the stiffness matrix, $\boldsymbol{\tau}_d$ is the disturbance vector, $\boldsymbol{I}$ is

Received 28 December 2000; revision received 6 June 2003; accepted for publication 17 July 2003.

*Postdoctoral Appointee, Department 15211, P.O. Box 5800, Mail Stop 1003. Member AIAA.
†Professor, Department of Mechanical Engineering.
‡Associate Professor, Department of Mechanical Engineering–Engineering Mechanics, 1400 Townsend. Member AIAA.
§Manager II, Department 6200, P.O. Box 5800, Mail Stop 0741. Associate Fellow AIAA.

the identity matrix, $\boldsymbol{b}$ is the piezoceramic transmission matrix, $\boldsymbol{\tau}$ is the general motor torque vector, and $\boldsymbol{V}_{\text{piezo}}$ is the vector of voltage applied to the piezoceramic actuators.

In practice, flexible modes are usually not directly available as an output variable. For this development, it is assumed that strain gauge measurements $\boldsymbol{y}$ are available. The flexible mode generalized coordinates $\boldsymbol{q}_f$ are related to the strain measurements by $\boldsymbol{q}_f = \boldsymbol{C}_{fy}^{-1}\boldsymbol{y}$, where the invertability of $\boldsymbol{C}_{fy}$ is ensured through appropriate positioning of the strain gauges and assuming the number of sensors is the same as the number of modes to be controlled.

The flexible manipulator dynamics of Eq. (1) can be transformed into output measurement space[6] as

$$\tilde{\boldsymbol{M}}\begin{Bmatrix}\ddot{\boldsymbol{q}}_r\\ \ddot{\boldsymbol{y}}\end{Bmatrix} + \tilde{\boldsymbol{C}}\begin{Bmatrix}\dot{\boldsymbol{q}}_r\\ \dot{\boldsymbol{y}}\end{Bmatrix} + \tilde{\boldsymbol{D}}\begin{Bmatrix}\dot{\boldsymbol{q}}_r\\ \dot{\boldsymbol{y}}\end{Bmatrix} + \tilde{\boldsymbol{K}}\begin{Bmatrix}\boldsymbol{q}_r\\ \boldsymbol{y}\end{Bmatrix} + \boldsymbol{\Omega}^T\begin{Bmatrix}\boldsymbol{\tau}_{d_r}\\ \boldsymbol{\tau}_{d_f}\end{Bmatrix} = \boldsymbol{\Omega}^T\begin{bmatrix}\boldsymbol{I} & \boldsymbol{0}\\ \boldsymbol{0} & \boldsymbol{b}\end{bmatrix}\begin{Bmatrix}\boldsymbol{\tau}\\ \boldsymbol{V}_{\text{piezo}}\end{Bmatrix} \tag{2}$$

where $\tilde{\boldsymbol{M}} = \boldsymbol{\Omega}^T\boldsymbol{M}\boldsymbol{\Omega}$, $\tilde{\boldsymbol{C}} = \boldsymbol{\Omega}^T\boldsymbol{C}\boldsymbol{\Omega}$, $\tilde{\boldsymbol{D}} = \boldsymbol{\Omega}^T\boldsymbol{D}\boldsymbol{\Omega}$, $\tilde{\boldsymbol{K}} = \boldsymbol{\Omega}^T\boldsymbol{K}\boldsymbol{\Omega}$, and $\boldsymbol{\Omega} = \text{diag}[\boldsymbol{I}, \boldsymbol{C}_{fy}^{-1}]$. The skew symmetric property still applies in the sense that for $\boldsymbol{x}^T(\dot{\boldsymbol{M}} - 2\boldsymbol{C})\boldsymbol{x} = 0, \forall x \in R^n$, the same holds for $\tilde{\boldsymbol{M}}$ and $\tilde{\boldsymbol{C}}$ because $\boldsymbol{x}^T(\dot{\tilde{\boldsymbol{M}}} - 2\tilde{\boldsymbol{C}})\boldsymbol{x} = \boldsymbol{x}^T\boldsymbol{\Omega}^T(\dot{\boldsymbol{M}} - 2\boldsymbol{C})\boldsymbol{\Omega}\boldsymbol{x} = (\boldsymbol{\Omega}\boldsymbol{x})^T(\dot{\boldsymbol{M}} - 2\boldsymbol{C})(\boldsymbol{\Omega}\boldsymbol{x}) = 0, \forall \boldsymbol{x} \in R^n$.

III. NAC Design

In this section a NAC law is designed based on Lyapunov's direct method. The desired angle trajectory and derivatives are denoted as $\boldsymbol{q}_{r_d}(t)$, $\dot{\boldsymbol{q}}_{r_d}(t)$, and $\ddot{\boldsymbol{q}}_{r_d}(t)$, respectively. The desired strain trajectory and derivatives are considered zero because the objective is to minimize vibration. The following error signals are defined as $\boldsymbol{e} = [\boldsymbol{e}_r \quad \boldsymbol{e}_f]^T$, where $\boldsymbol{e}_r = (\boldsymbol{q}_{r_d} - \boldsymbol{q}_r)$ and $\boldsymbol{e}_f = (\boldsymbol{0} - \boldsymbol{y})$, respectively. The tracking error sliding surface is defined as

$$\boldsymbol{S} = \dot{\boldsymbol{e}} + \boldsymbol{\Lambda}\boldsymbol{e} + \boldsymbol{\Psi}\int \boldsymbol{e}\,\mathrm{d}t = \begin{bmatrix}\dot{\boldsymbol{e}}_r + \boldsymbol{\lambda}_r\boldsymbol{e}_r + \boldsymbol{\psi}_r\int \boldsymbol{e}_r\,\mathrm{d}t\\ \dot{\boldsymbol{e}}_f + \boldsymbol{\lambda}_f\boldsymbol{e}_f + \boldsymbol{\psi}_f\int \boldsymbol{e}_f\,\mathrm{d}t\end{bmatrix} = \begin{bmatrix}\boldsymbol{s}_r\\ \boldsymbol{s}_f\end{bmatrix} \tag{3}$$

where $\boldsymbol{\Lambda}$ and $\boldsymbol{\Psi}$ are both diagonal positive definite matrices. The dynamic equations [Eq. (2)] are expressed in terms of $\boldsymbol{S}$ (Ref. 8) as

$$\tilde{\boldsymbol{M}}\dot{\boldsymbol{S}} + \tilde{\boldsymbol{C}}\boldsymbol{S} + \tilde{\boldsymbol{D}}\boldsymbol{S} = \boldsymbol{Y}(\cdot)\boldsymbol{\varphi} - \begin{Bmatrix}\boldsymbol{\tau}\\ \boldsymbol{C}_{fy}^{-1}\boldsymbol{b}\boldsymbol{V}_{\text{piezo}}\end{Bmatrix} + \begin{Bmatrix}\boldsymbol{\tau}_{d_r}\\ \boldsymbol{C}_{fy}^{-1}\boldsymbol{\tau}_{d_f}\end{Bmatrix} \tag{4}$$

where

$$\boldsymbol{Y}(\cdot)\boldsymbol{\varphi} = \begin{bmatrix}\boldsymbol{Y}_r(\cdot)\boldsymbol{\varphi}_r\\ --\ --\\ \boldsymbol{Y}_f(\cdot)\boldsymbol{\varphi}_f\end{bmatrix} = \begin{bmatrix}\boldsymbol{M}_{rr}\left(\ddot{\boldsymbol{q}}_{r_d} + \boldsymbol{\lambda}_r\dot{\boldsymbol{e}}_r + \boldsymbol{\psi}_r\boldsymbol{e}_r\right) + \boldsymbol{M}_{rf}(\boldsymbol{\lambda}_f\dot{\boldsymbol{e}}_f + \boldsymbol{\psi}_f\boldsymbol{e}_f)\\ \quad + \boldsymbol{C}_{rr}\left(\dot{\boldsymbol{q}}_{r_d} + \boldsymbol{\lambda}_r\boldsymbol{e}_r + \boldsymbol{\lambda}_r\int \boldsymbol{e}_r\,\mathrm{d}t\right) + \boldsymbol{C}_{rf}\left(\boldsymbol{\lambda}_f\boldsymbol{e}_f + \boldsymbol{\psi}\int \boldsymbol{e}_f\,\mathrm{d}t\right)\\ \quad + \boldsymbol{D}_{rr}\left(\dot{\boldsymbol{q}}_{r_d} + \boldsymbol{\lambda}_r\boldsymbol{e}_r + \boldsymbol{\psi}_r\int \boldsymbol{e}_r\,\mathrm{d}t\right)\\ ---------- \\ \boldsymbol{M}_{fr}\left(\ddot{\boldsymbol{q}}_{r_d} + \boldsymbol{\lambda}_r\dot{\boldsymbol{e}}_r + \boldsymbol{\psi}_r\boldsymbol{e}_r\right) + \boldsymbol{M}_{ff}(\boldsymbol{\lambda}_f\dot{\boldsymbol{e}}_f + \boldsymbol{\psi}_f\boldsymbol{e}_f)\\ \quad + \boldsymbol{C}_{fr}\left(\dot{\boldsymbol{q}}_{r_d} + \boldsymbol{\lambda}_r\boldsymbol{e}_r + \boldsymbol{\psi}_r\int \boldsymbol{e}_r\,\mathrm{d}t\right) + \boldsymbol{C}_{ff}\left(\boldsymbol{\lambda}_f\boldsymbol{e}_f + \boldsymbol{\psi}_f\int \boldsymbol{e}_f\,\mathrm{d}t\right)\\ \quad - \boldsymbol{K}_F\boldsymbol{e}_f\end{bmatrix} \tag{5}$$

Note that $\boldsymbol{Y}(\cdot)$ is a regression matrix that depends only on known time functions of actual and desired trajectories and $\boldsymbol{\varphi}$ is a vector of unknown constant parameters.

The following positive Lyapunov candidate function (see Refs. 4 and 8) is selected as

$$V(t) = \tfrac{1}{2}\boldsymbol{S}^T\tilde{\boldsymbol{M}}\boldsymbol{S} + \tfrac{1}{2}\tilde{\boldsymbol{\varphi}}^T\boldsymbol{\Gamma}^{-1}\tilde{\boldsymbol{\varphi}} \tag{6}$$

where $\boldsymbol{\Gamma}^{-1}$ is a constant, symmetric matrix. The stability requirement of $\dot{V} \le 0$ is examined by considering the expression for $\dot{V}$:

$$\dot{V}(t) = \boldsymbol{S}^T\left[\boldsymbol{Y}(\cdot)\boldsymbol{\varphi} - \begin{Bmatrix}\boldsymbol{\tau}\\ \boldsymbol{C}_{fy}^{-1}\boldsymbol{b}\boldsymbol{V}_{\text{piezo}}\end{Bmatrix} + \begin{Bmatrix}\boldsymbol{\tau}_{d_r}\\ \boldsymbol{C}_{fy}^{-1}\boldsymbol{\tau}_{d_f}\end{Bmatrix}\right] - \boldsymbol{S}^T\tilde{\boldsymbol{D}}\boldsymbol{S} + \tilde{\boldsymbol{\varphi}}^T\boldsymbol{\Gamma}^{-1}\dot{\tilde{\boldsymbol{\varphi}}} \tag{7}$$

The following nonlinear model-based control laws are postulated in matrix form[8] as

$$\begin{Bmatrix}\boldsymbol{\tau}\\ \boldsymbol{C}_{fy}^{-1}\boldsymbol{b}\boldsymbol{V}_{\text{piezo}}\end{Bmatrix} = \boldsymbol{Y}(\cdot)\hat{\boldsymbol{\varphi}} + \boldsymbol{K}_v\boldsymbol{S} + \boldsymbol{A}\,\text{sgn}(\boldsymbol{S}) \tag{8}$$

where $\hat{\boldsymbol{\varphi}}$ is the estimate of $\boldsymbol{\varphi}$. Substitution of Eq. (8) into Eq. (7) gives

$$\dot{V} = -\boldsymbol{S}^T\boldsymbol{K}_v\boldsymbol{S} - \boldsymbol{S}^T\tilde{\boldsymbol{D}}\boldsymbol{S} - \boldsymbol{S}^T[\boldsymbol{A}\,\text{sgn}(\boldsymbol{S}) - \boldsymbol{\tau}_d] + \tilde{\boldsymbol{\varphi}}^T[\boldsymbol{Y}^T(\cdot)\boldsymbol{S} + \boldsymbol{\Gamma}^{-1}\dot{\tilde{\boldsymbol{\varphi}}}] \tag{9}$$

where $\tilde{\boldsymbol{\varphi}} = \boldsymbol{\varphi} - \hat{\boldsymbol{\varphi}}$. To achieve Lyapunov stability, $\dot{V} \le 0$, the following deductions are made: The controller gain matrix $\boldsymbol{K}_v$ must be positive definite, the physical plant damping matrix $\boldsymbol{D}$ is positive definite, and for disturbance rejection the following constraint must hold, $\boldsymbol{A} > \max\{|\boldsymbol{\tau}_d|\}$, where $\boldsymbol{A}$ is a positive-definite controller gain matrix. The adaptive update equations are determined by setting the coefficient inside the last term of Eq. (9) to zero and solve for the general adaptive update equations[4,8] as

$$\dot{\hat{\boldsymbol{\varphi}}} = \boldsymbol{\Gamma}\boldsymbol{Y}^T(\cdot)\boldsymbol{S} \tag{10}$$

where $\boldsymbol{\varphi}$ is constant. Under these conditions, the system is stable. In a manner similar to Lewis et al.,[5] it can be shown that the tracking error $\boldsymbol{e}$ is asymptotically stable, whereas the velocity tracking error $\dot{\boldsymbol{e}}$ and parameter estimates $\boldsymbol{\varphi}$ are bounded.

The NAC architecture was implemented on a slewing active structure. The active structure was designed and built using graphite/epoxy prepreg composite laminates.[9] The composite design and layup using an across the centerline symmetric layup is shown in Fig. 1. Piezoceramic actuators and strain gauge sensors were embedded, as indicated, between 0-angle plies. To increase the structure's torsional stiffness ±45-deg angle plies were inserted. This design option is not available when using standard homogeneous materials. The strain actuators and sensors were embedded at the end of the composite link to maximize induced strain for a cantilever boundary condition. An electrical connector was used to terminate all actuator and sensor signals that exit at the end of the structure. The specific structural geometric dimensions and piezoceramic properties are listed in Tables 1 and 2. The piezoceramic actuator patches are placed symmetrically across the neutral axis and are connected electrically 180-deg out-of-phase so that as one contracts the other expands, resulting in a moment $M(x, t)$ applied to the flexible link.

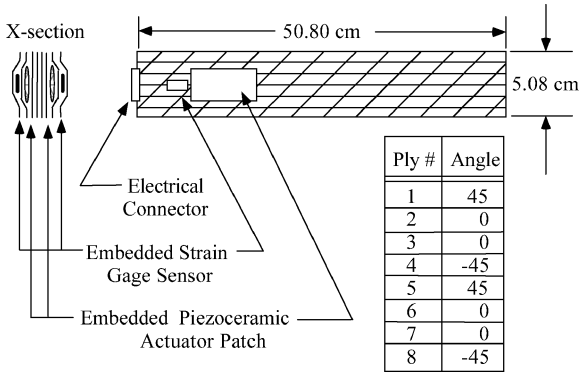

Ply #	Angle
1	45
2	0
3	0
4	-45
5	45
6	0
7	0
8	-45

Fig. 1 Active link laminate design.

Table 1 Flexible active structure properties

Beam parameters	Symbol	Value	Unit
Length	L	44.61	cm
Width	w	5.08	cm
Thickness	t	0.1829	cm
Hub radius	r	0.635	cm
Mass density	ρ_m	1522	kg/m^3
Tip mass	M_t	0.022	kg
Beam stiffness	EI	0.9985	N $\cdot$ m^2
Gear ratio	N	100	

Table 2 Piezoceramic actuator properties

Piezoceramic parameters	Symbol	Value	Unit
Lateral strain coefficient	d_{31}	-180.0	pm/V
Axial strain coefficient	d_{33}	360.0	pm/V
Young's modulus	E_{piezo}	63.0	GPa
Mass density	ρ_{piezo}	7650	kg/m^3
Piezoceramic wafer length	L_{piezo}	5.5974	cm
Piezoceramic wafer width	w_{piezo}	3.3274	cm
Piezoceramic wafer thickness	t_{piezo}	0.0254	cm
Capacitance	C	0.01	μF
Voltage range	V	± 200	V

For the piezoceramic beam actuator, only the residual vibrations after the slew maneuver are of concern. The sgn(s) was approximated by tanh(βs) function, where β defines the steepness of the saturation slope. This boundary layer provided a smooth transition and minimized the effects of chatter. For $n_r = n_f = 1$, the following single-mode control algorithms are defined as

$$\tau = \boldsymbol{Y}_r(\cdot)\hat{\boldsymbol{\varphi}}_r + K_{v_r} s_r + A_r \tanh(\beta_r s_r) + \tau_{LR} \tag{11}$$

and for the flexible partition,

$$C_{fy}^{-1} b V_{\text{piezo}} = \boldsymbol{Y}_f(\cdot)\hat{\boldsymbol{\varphi}}_f + K_{v_f} s_f + A_f \tanh(\beta_f s_f) \tag{12}$$

where $\boldsymbol{Y}_r(\cdot)\hat{\boldsymbol{\varphi}}_r$ and $\boldsymbol{Y}_f(\cdot)\hat{\boldsymbol{\varphi}}_f$ were defined earlier and, for a single mode, do not have any nonlinear coupling Coriolis/centripetal terms. In Eq. (11) the term τ_{LR} is a corrective term used to preserve the passivity properties. For flexible joint systems, Spong[10] first introduced the following coupling control term:

$$\tau_{LR} = K_{LR}(\dot{q}_L - \dot{q}_R) \tag{13}$$

which is added to flexible joint manipulators to maintain the same passivity properties as rigid-joint manipulators. The subscripts L and R represent link and rotor velocities, respectively. This term requires velocity measurements on both the motor and link sides, where K_{LR} is a positive controller gain. The adaptive update equations are defined for five unique parameters as $\hat{\hat{m}}_{rr} = \gamma_1 Y_{11} s_r$, $\hat{\hat{m}}_{rf} = \gamma_2(Y_{12} s_r + Y_{11} s_f)$, $\hat{\hat{d}}_{rr} = \gamma_3 Y_{13} s_r$, $\hat{\hat{m}}_{ff} = \gamma_4 Y_{12} s_f$, and $\hat{\hat{k}}_F = \gamma_5 Y_{14} s_f$, where Y_{ij} are part of the regression matrix and γ_i are the adaptation controller gains.

IV. Experimental Results

In this section experimental results are presented for which the NAC architecture was evaluated with and without active vibration control. The robustness of the controller algorithms were illustrated by increasing the tip mass from 0.002 kg (nominal) to 0.022 kg. All of the controller gains were selected based on previously developed stability criteria. The testbed consists of an encoder, dc motor, and harmonic drive actuator assembly. This servoactuator is nonbackdriveable, which requires residual vibrations to be absorbed by beam actuation. The servoactuator is very popular in many robotic applications where servo positioning is the premise. A MATLAB®/dSPACE control/data acquisition architecture provided a rapid prototyping environment. The piezoceramic actuator was located near the root of the link to target vibration suppression of the first-mode bending frequency, at 7.0 Hz. For higher bending modes, additional strain

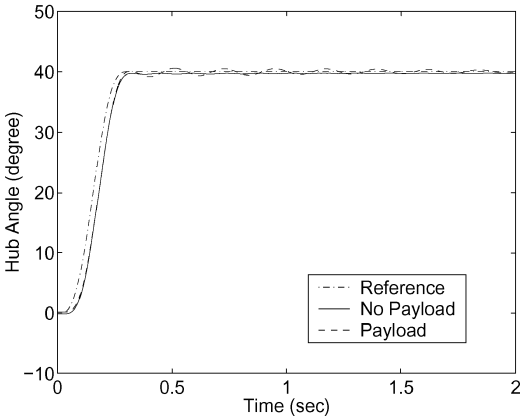

a) Hub angle slew responses

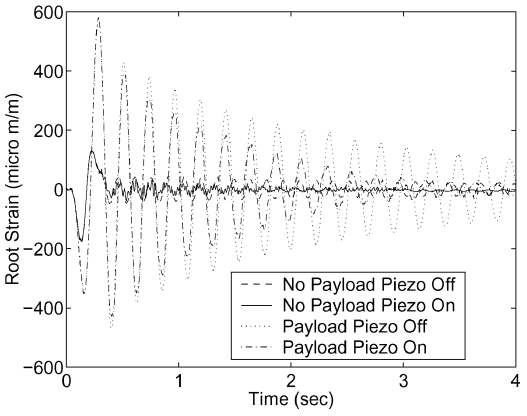

b) Root strain responses

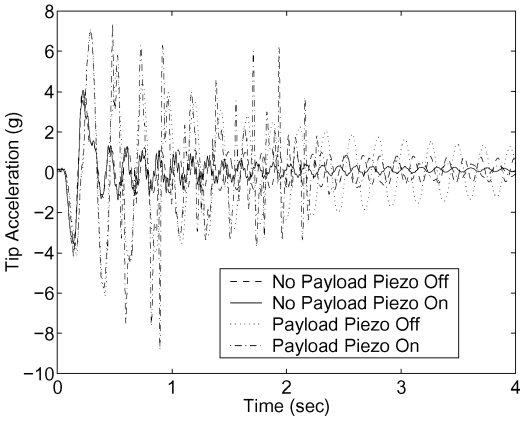

c) Tip acceleration responses

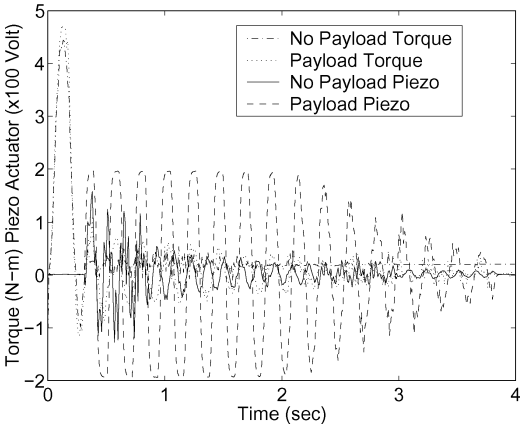

d) Slewing link inputs

Fig. 2 Experimental nonlinear adaptive control results.

actuators and sensors would need to be appropriately located and added to the active structure. The strain-rate estimate was generated with a band-limited derivative filter, with the cutoff frequency set to 20 Hz. The filter captured the derivative estimation of the targeted first-mode bending frequency.

The slewing active structure was subjected to a near-minimum time input[11] from 0 to 40 deg in 0.317 s. Two runs were performed both with and without a payload variation. In addition, each run was performed with and without active vibration control. The reference trajectory, passive (piezo off) and active (piezo on) runs for the no-payload case are shown in Fig. 2. The slew trajectory was tracked very well with small oscillations. The root strain responses are shown in Fig. 2. With the active case, the initial residual strain was reduced by 10–15 μstrain and the settling time reduced, from greater than 10 to less than 3 s. The tip acceleration reponses are shown in Fig. 2, which demonstrate similar reductions in settling time.

The NAC algorithm was tested for robustness to parameter variations by increasing the tip mass, which reduced the first bending frequency to 4.5 Hz. The results for this run are also shown in Fig. 2. For the angle responses, the control algorithm still maintained good tracking performance with an increase in oscillations about the set point. It is believed that the piezoceramic actuator saturation does not allow the controllers to be completely decoupled. The oscillations in Fig. 2, caused by the tip mass variation, do not persist and die out after 3 s. With the tip mass variation, a similar reduction in settling time and residual vibrations are still observed for the active run. For the acceleration response, residual vibrations and settling time are reduced for time greater than 2 s; however, the increased transient spikes are due to piezoceramic actuator saturation. Reduction in these transients would require an increase in piezoceramic actuator control authority. The corresponding motor torque and piezoceramic actuator voltages for with and without a payload are shown in Fig. 2. A 50% amplitude reduction for the piezoceramic actuator was applied to prevent degradation due to large actuation voltages relative to lower vibration levels. This problem is reviewed in more detail in Ref. 12.

V. Conclusions

A robust NAC system was designed for the rotational slewing of an active structure. Experimental runs validated the control system performance. Reductions in both residual vibration and settling time resulted. Robustness to parameter variations were tested by increasing the tip mass so that the first-mode bending frequency was reduced. Control system performance results were similar to the zero tip mass case.

Acknowledgments

Sandia National Laboratories is a multiprogram laboratory operated by Sandia Corporation, a Lockheed Martin Company, for the U.S. Department of Energy under Contract DE-AC0494AL-85000. The first author was also supported through WAYA Research, Inc. Special thanks are given to Roy Ikegami and his technical team at The Boeing Company Phantom Works, Structures Technology Department, Kent, Washington for their internal research and development support and creation of the composite active structures.

References

[1]Inman, D. J., Garcia, E., and Pokines, B., "Issues in Slewing an Active Structure," *Proceedings of the US–Japan Workshop on Smart/Intelligent Materials and Systems*, Honolulu, Hawaii, 1990, pp. 199–210.

[2]Denoyer, K. K., and Kwak, M. K., "Dynamic Modelling and Vibration Suppression of a Slewing Structure Utilizing Piezoelectric Sensors and Actuators," *Journal of Sound and Vibration*, Vol. 189, No. 1, 1996, pp. 13–31.

[3]Choi, S. B., and Shin, H. C., "A Hybrid Actuator Scheme for Robust Position Control of a Flexible Single-Link Manipulator," *Journal of Robotic Systems*, Vol. 13, No. 6, 1996, pp. 359–370.

[4]Slotine, J.-J. E., and Li, W., *Applied Nonlinear Control*, Prentice–Hall, Englewood Cliffs, NJ, 1991, Chaps. 8, 9.

[5]Lewis, F. L., Abdallah, C. T., and Dawson, D. M., *Control of Robot Manipulators*, Macmillan, New York, 1993, Chaps. 5, 6.

[6]Yang, J., Lian, F., and Fu, L., "Adaptive Robust Control for Flexible Manipulators," *Proceedings of the IEEE Conference on Robotics and Automation*, 1995, IEEE Publications, Piscataway, NJ, pp. 1223–1228.

[7]Yang, J., Lian, F., and Fu, L., "Nonlinear Adaptive Control for Flexible-Link Manipulators," *IEEE Transactions on Robotics and Automation,* Vol. 11, No. 1, 1997, pp. 140–148.

[8]Wilson, D. G., "Nonlinear/Adaptive Control Architectures with Active Structures for Flexible Manipulators," Ph.D. Dissertation, Mechanical Engineering, Univ. of New Mexico, Albuquerque, NM, May 2000.

[9]Wilson, D. G., Searle, I., Ikegami, R., and Starr, G. P., "Dynamic Characterization of Smart Structures for Active Vibration Control Applications," *Proceedings of the ASME Noise Control and Acoustics Division*, Vol. 2, American Society of Mechanical Engineers, Fairfield, NJ, 1996, pp. 29–35.

[10]Spong, M. W., "Adaptive Control of Flexible Joint Manipulators," *Systems and Control Letters*, Vol. 13, No. 1, 1989, pp. 15–21.

[11]Junkins, J. L., Rahman, Z. H., and Bang, H., "Near-Minimum-Time Control of Distributed Parameter Systems: Analytical and Experimental Results," *Journal of Guidance, Control, and Dynamics,* Vol. 14, No. 2, 1991, pp. 406–415.

[12]Choi, S. B., Cheong, C. C., and Kim, S. H., "Control of Flexible Structures by Distributed Piezofilm Actuators and Sensors," *Journal of Intelligent Material Systems and Structures*, Vol. 6, May 1995, pp. 430–435.

Partial Eigenstructure Assignment Approach for Robust Flight Control

Atsushi Satoh* and Kenji Sugimoto†
Nara Institute of Science and Technology, Nara 630-0192, Japan

Introduction

THE main purpose of a flight control system is to improve the aircraft's dynamic properties for good flying quality. For example, the well-known MIL-F-8785C (Ref. 1) gives some performance criteria for good flying quality. In this guidance, the criteria are translated into the eigenstructure specifications. Therefore, eigenstructure assignment[2,3] is particularly suitable for attaining good transient responses, and many successful applications for flight control design are presented.[4–9]

At the same time, an implemented control system should not cause instability, even though there exist parameter uncertainties, unmodeled dynamics, and so forth. However, feedback synthesis with a given robustness bound via ordinary eigenstructure assignment technique is a difficult problem, because little design freedom is left for achieving another objective such as robust stabilization.

To attain more design freedom, partial pole/eigenstructure assignment[10–16] is an effective technique. In the pioneering work,[10,11,14] pole placement of large-scale systems and eigenvalue sensitivity improvement by attained freedom are primarily considered. The dynamic properties of aircraft fundamentally consist of rigid-body dynamics and parasitic dynamics (e.g., washout filter, actuator dynamics, etc.); the former predominantly affects flying quality. Therefore, partial eigenstructure assignment is a reasonable approach. Kim and Kim[15] reduced the attained freedom to a design parameter via the null space approach and discussed an application to flight control design by linear quadratic regulator with partial eigenstructure assignment.

Received 14 November 2002; revision received 23 June 2003; accepted for publication 12 August 2003.

*Assistant Professor, Graduate School of Information Science; s-atushi@is.aist-nara.ac.jp.

†Professor, Graduate School of Information Science; kenji@is.aist-nara.ac.jp.